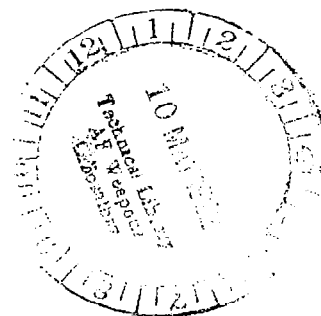NASA Contractor Report 3521

Studies of Single-Mode Injection Lasers and of Quaternary Materials

Volume II - Measurement of Electro-Optic Effects in InGaAsP Junction Waveguides

Jacob M. Hammer

NASA

NASA Contractor Report 3521

Studies of Single-Mode Injection Lasers and of Quaternary Materials

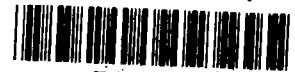## Volume II - Measurement of Electro-Optic Effects in InGaAsP Junction Waveguides

Jacob M. Hammer
RCA Laboratories
Princeton, New Jersey

NASA

National Aeronautics
and Space Administration

Scientific and Technical
Information Branch

1982

PREFACE

This Final Report covers work performed at RCA Laboratories during the period 4 February 1980 to 15 May 1981 under Contract No. NAS1-15440. This work was carried out in the Solid State Devices Laboratory, under the direction of B. Hershenov. The Group Head was M. Ettenberg, and the Project Scientist was I. Ladany. (Volume I of this report was written by D. Botez and Volume II by J. M. Hammer.) Staff members and support personnel who contributed to this work in addition to the authors, and the area of their contribution, are listed below:

J. C. Connolly	-	LPE growth
D. Gilbert	-	Device characterization
M. Harvey	-	Device processing
H. Kowger	-	Facet coating
D. P. Marinelli	-	Device processing
C. C. Neal	-	Coupling measurements, lens and prism mount design

TABLE OF CONTENTS

Section

SUMMARY

We have measured both the linear electro-optic (Pockel's) effect and electroabsorption (Franz-Keldysh effect) in waveguiding junctions of InGaAsP. With our data and a field overlap theory, the electro-optic coefficient r_{41} is found to be $0.1-0.14 \times 10^{-12}$ m/V at $\lambda = 1.54 - 1.65$ μm. To the best of our knowledge this is the first reported measurement of the electro-optic coefficient for InGaAsP.

We have also measured the electroabsorption and found a value on the order of 7×10^{-4} cm^{-1}/(V/cm) or approximately 100 cm^{-1} for fields of 2×10^5 V/cm at $\lambda \sim$ 1.3 μm. All measurements were made on a quaternary film with a bandgap wavelength of 1.23 μm.

Because of the rapid commercial introduction of quaternary lasers, LEDs, and detectors to take advantage of large optical fiber bandwidths and low losses in the 1.2- to 1.7-μm region, these measurements are significant in providing some of the basic physical constants needed to design modulators and switches capable of operating at microwave frequencies in this wavelength region.

I. INTRODUCTION

The purpose of this contract is the study of electric-field-induced effects in the waveguiding properties of InGaAsP junctions. The 1.2- to 1.7-μm wavelength region has high technological interest for optical communications because of the low optical fiber loss and large fiber optical bandwidth observed in this region. Quaternary LEDs, lasers, and detectors operating in this region are rapidly being developed to a state of commercial application. This study is designed to observe electric-field-induced phenomena such as the linear electro-optic (Pockel's) and electroabsorption (Franz-Keldysh) effects that may play a role in using quaternary junctions not only as sources and detectors but possibly as modulators and/or switches capable of operating in the microwave region (refs. 1,2).

Since InGaAsP is not available as a bulk material, we have developed both the necessary theoretical descriptions and experimental techniques to make measurements on the quaternary films which enable the extraction of the linear electro-optic coefficient r_{41} and a coefficient α_f which describes the field-induced loss due to electroabsorption.

Laser light from a quaternary laser at λ_1 is end fired into the junction plane of a second laser designed to operate at $\lambda_2 < \lambda_1$. The near-field light emerging from the end of the InP-InGaAsP-InP waveguide of the second laser is studied in the image plane. We will refer to the laser being studied as the modulator. The modulator is operated in reverse bias to observe the electro-optic effects. (The modulator bandgap wavelength is $\lambda_2 = 1.23$ μm for all measurements.)

In the linear electro-optic measurements the plane of the laser is set at 45° to the plane of the waveguide and a polarization analyzer interposed between the near-field image detector and the waveguide. Here, the ac signal under pulsed reverse bias is related to the electro-optic coefficient. Also, in agreement with theory, the signal varies linearly with reverse bias voltage in the 0- to 6.0-V range used. These measurements are made with source lasers at $\lambda = 1.65$ μm and 1.54 μm.

Electroabsorption measurements are made using a source laser at $\lambda_1 = 1.30$ μm. Here the strong absorption effect observed in back bias obscures the electro-optic effect. For the absorption measurements the modulator is pulsed

in reverse bias and the ac signal at selected transverse positions of the near-field image recorded. Reverse bias results in a reduction of transmission at the peak of the image. The reduction is an exponential function of bias voltage and is attributed to the Franz-Keldysh effect.

The measurements on electroabsorption in InGaAsP by Kingston (ref. 3) were restricted to transmission perpendicular to the junction plane. The theory necessary to describe the measurements and extract the significant physical quantities is developed in Section II. The method is described in Section III, the experimental results in Section IV. Section V is a discussion of the measurements, and our conclusions are given in Section VI.

II. THEORY

A. GENERAL DESCRIPTION

We consider light traveling in a waveguide mode of the structure shown in Figure 1. The thicknesses, doping, and refractive indexes of the layers are shown in the figure. The details of the growth and use of structures similar to these as lasers and LEDs are given in references 4 and 5. The high-refractive-index (n = 3.5) InGaAsP N⁻ layer is surrounded by InP layers with refractive indexes n ~ 3.2. This structure forms a single-mode-symmetric-planar-optical waveguide for light traveling in the Z direction. A sketch of the modal field is also shown in Figure 1. For TE (TM) modes the electric (magnetic) vector is parallel to the Y axis. If a negative voltage V is applied to the P contact (back bias), as is well-known (ref. 6) a depletion layer will form in the region of the junction and an electric field will exist in this region. The electric field will indirectly affect the propagation of the waveguide mode through two mechanisms. For TE modes the electric field can cause phase velocity changes due to the linear electro-optic (Pockel's) effect acting through the r_{41} electro-optic coefficient. This is the coefficient appropriate to the class of crystal symmetry of zinc-blend structures [guide plane (001) light enters along (110) TE waves, ref. 7]. In addition, electro-absorption (Franz-Keldysh) effects will also be observed for either TE or TM waves.

We will first discuss Pockel's effect. If a plane wave, y polarization, completely fills a crystal satisfying the same symmetry condition as our waveguide and the crystal contains an x component of electric field E, the refractive index of the crystal will change by an amount $\Delta n = -n^3 r_{41} E/2$ and the phase of the wave in traveling a distance L in the Z direction will change by

$$\Delta\phi = \frac{2\pi L}{\lambda_0} \Delta n$$

or

$$\Delta\phi = \frac{\pi L n^3 r_{41}}{\lambda_0} E \qquad (1)$$

If plane-polarized light enters the crystal with the plane of polarization tilted at 45° to the x axis, the emerging light will in general be elliptically
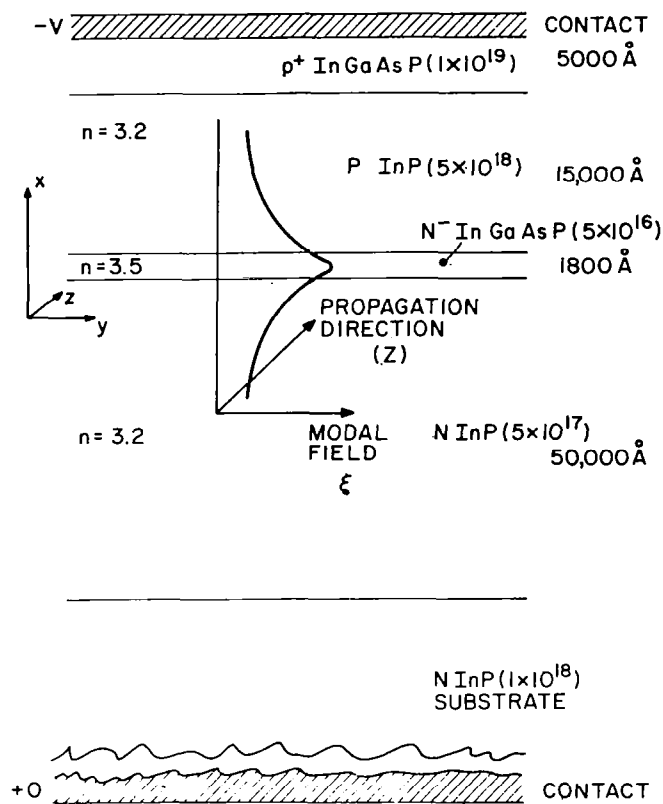
Figure 1. Cross section through modulator sample. The waveguide modal
field distribution is sketched in the center of the figure.
A negative voltage at the p$^+$ contact with respect to the N
contact puts the N$^-$ InGaAsP "active" layer in back bias.

polarized. The portion of the light with electric-field-induced ellipticity
will emerge from a polarization analyzer with an intensity given by

$$I = I_0 \sin^2 \Delta\phi/2 \tag{2}$$

where I_0 is the intensity entering the analyzer (ref. 8). Thus, by measuring
the intensity variation of light passing through both the crystal and a polari-
zation analyzer as a function of the applied field, it is possible to find the
electro-optic coefficient using equations (1) and (2). This method can also be
applied to propagation of a waveguide mode through our structure. Here,
however, the nonuniformity of the applied electric field and the electric field

distribution of the guided mode must be taken into account. This will be done below by evaluating the overlap integral between the junction depletion field and the waveguide mode.

We first consider the character of the applied electric field in the junction region. An enlarged sketch of the depletion fields (solid lines) and the waveguide modal field (dashed lines) is shown in Figure 2. The expressions for these fields are derived below. The applied field (denoted by E) is partially pinned in the low conductivity quaternary layer ($N^- = 5 \times 10^{16}$ cm^3). There is, however, substantial tailing into the N InP region (5×10^{17} cm^3). Thus, the overlap between the applied and waveguide fields must include this region.
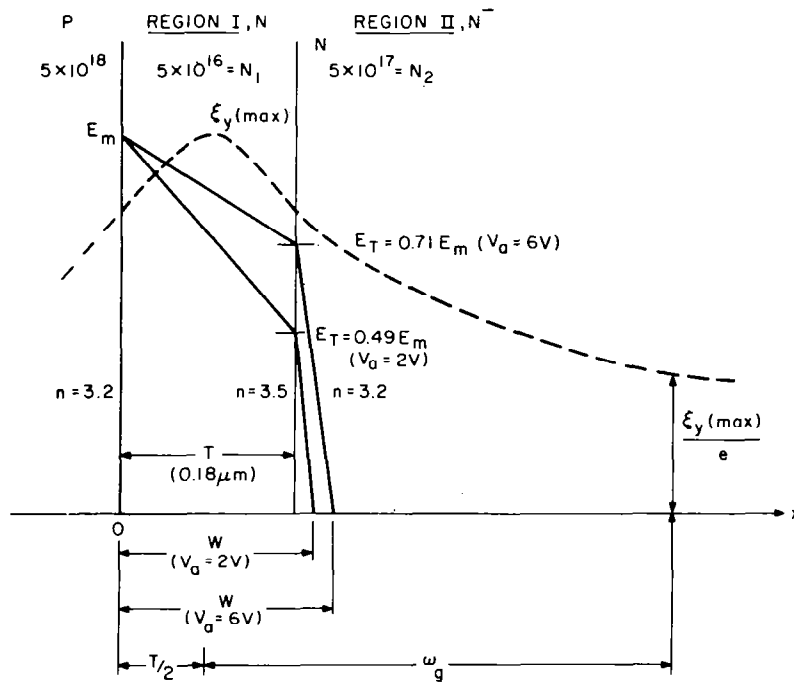

Figure 2.   Enlarged cross section of modulator in active-layer region. The depletion-layer fields $E(x)$ are shown as solid lines. The waveguide modal field ξ_y is shown as a dashed line. The modal field falls to $1/e$ of its maximum value at a distance from the p-n junction of $\omega_g + T/2$.

B. FIELDS IN JUNCTION REGION

The applied field behavior is derived as follows. We use Poisson's equation $\nabla^2 V = -\rho/\varepsilon$ where ρ is the charge density eN, e is the electronic charge, and N is the density of free carriers. ε is the absolute dielectric constant $= \varepsilon'\varepsilon_0$. ε_0 is the permittivity of space (8.85×10^{-12} F/m). We assume that the potential V is a function only of x. Using $E(x) = -\partial V/dx$, we look for solutions of

$$\partial E/\partial x = \frac{Ne}{\varepsilon} \tag{3}$$

For the case of abrupt junctions, a general solution is $E(x) = Ax+B$. We apply the boundary conditions at $x = 0$, $E = E_m$ and at $x = T$, $E = E_T$. The solutions are

$$\text{Region I} \qquad E(x) = \left(\frac{E_T - E_m}{T}\right) x + E_m \quad \text{and} \tag{4a}$$

$$\text{Region II} \qquad E(x) = \frac{E_T}{T - W} (x - W) \tag{4b}$$

We are ignoring any field penetration into the more highly doped P region (5×10^{18}/cm^3). From the second derivative $E = -\partial V/dx$ we obtain the general solution

$$V = A_3 x^2 + B_3 x + C_3 \tag{5}$$

The boundary conditions here are

$$\text{at } x = W, \qquad E = V = 0$$
and $\tag{6}$
$$\text{at } x = 0, \qquad -V = V_a + V_{BI}$$

The built-in potential V_{BI} is discussed by S.M. Sze (ref. 6) and is expected to have a value close to that for GaP, $V_{BI} \sim 1.35$ V. Using equations (4), (5),

(6) and the boundary condition in conjunction with $\partial E/\partial x = e/\varepsilon \, N_1$ in Region I and $\partial E/\partial x = e/\varepsilon \, N_2$ in Region II, we obtain

$$E_T = (e/\varepsilon) \, N_2 (T - W) \tag{7}$$

$$E_m = (e/\varepsilon)[(N_2 - N_1)T - N_2 W] \tag{8}$$

and

$$W = \sqrt{\frac{T^2(N_2 - N_1)}{N_2} + \frac{2\varepsilon}{eN_2}(V_{BI} + V_a)} \tag{9}$$

The fields shown in Figure 2 are plotted for the case, applicable to our measurements, of $N_1 = 5\times10^{16}/cm^3 = 5\times10^{22}/m^3$, $N_2 = 5\times10^{17}/cm^3 = 5\times10^{23}/m^3$. $V_{BI} = 1.35$ V, $\varepsilon = 13\varepsilon_0$, e (electronic charge) $= 1.6\times10^{-19}$ coulombs, $T = 0.18$ μm $= 0.18\times10^{-6}$ m, and for $V_a = 2$ and $V_a = 6$ V.

C. WAVEGUIDE MODES

As is well known, the solution for the electric field vector ξ_y of a mode for a step-index symmetric waveguide is a cosine function in the film region (high index n = 3.5) and a decaying exponential outside this region (low index n = 3.2). The mode width w_g, measured to the point at which ξ_y has fallen to 1/e of its maximum value, is denoted w_g and is given by

$$2w_g = T + \frac{\lambda_0}{\pi}\left(\frac{1}{\sqrt{n_g^2 - n_2^2}}\right)\left[1 + \ln\sqrt{\frac{n_1^2 - n_g^2}{n_g^2 - n_2^2}}\right] \tag{10}$$

where n_g is the equivalent refractive index of the guided mode obtained by solving the dispersion equation

$$\frac{2\pi T}{\lambda_0} = \frac{1}{\sqrt{n_1^2 - n_g^2}}\left(v\pi + 2\tan^{-1}\sqrt{\frac{n_g^2 - n_2^2}{n_1^2 - n_g^2}}\right) \tag{11}$$

8

Here ν is the mode number. $\nu = 0$ for the lowest order mode. For $T = 0.18$ μm, $\lambda_0 = 1.65$ μm, $n_1 = 3.5$, $n_2 = 3.2$, the lowest order mode width is found to be $w_g = 0.48$ μm. At $\lambda_0 = 1.298$, the wavelength used in the electroabsorption measurements, $w_g = 0.33$ μm. We represent the modal field as

(Region I)

$$\xi(x) = \xi_0 \cos\left(\frac{2\pi}{\lambda_0} \sqrt{n_1^2 - n_g^2} - \phi\right) x \quad \text{and} \tag{12a}$$

(Region II)

$$\xi(x) = \xi_0 \sqrt{\frac{n_1^2 - n_g^2}{n_1^2 - n_2^2}} \; \exp{-\frac{2\pi}{\lambda_0} \sqrt{n_g^2 - n_2^2} \; (x - T)} \tag{12b}$$

D. EFFECTIVE OVERLAP FIELD

To perform the convolution integral we formally represent the fields as follows:

	Region I	Region II
Waveguide Mode	$\xi = \xi_0 \cos(a_1 x + b_1)$	$\xi = \xi_0 b_2 \exp(-a_2 x)$
Applied Field	$E = A_1 x + B_1$	$E = A_2 x + B_2$

$$(13)$$

The effective applied field E_0 will be given by the overlap integrals

$$E_0 = \frac{1}{2w_g}\left[\int_0^T (A_1 x + B_1)\cos(a_1 x - b_1) \, dx \right.$$

$$\left. + \int_T^W (A_2 x + B_2) \exp(-a_2 x) dx \right] \tag{14}$$

Performing the indicated integrations, we find using equations (4a) and (4b):

$$E_0 = -\frac{e}{\varepsilon} \frac{T}{2w_g} N_2 \left[W(1 + b_2) + \frac{b_2 T^2}{W} + T \left(\frac{N_1}{2N_2} - 1 - 2b_2 \right) \right] \quad (15)$$

Note here that the dependence of the overlap field on applied voltage is contained only in the terms including W [see eq. (9)]. We are interested in the variation of electro-optic signal with V_a and, therefore, consider the derivative of the electro-optic signal with respect to V_a and obtain from equation (1)

$$\frac{d(I/I_0)}{dV_a} = 2 \left(\sin \frac{\Delta\phi}{2} \cos \frac{\Delta\phi}{2} \right) \frac{d\Delta\phi}{dV_a} \quad (16a)$$

For small $\Delta\phi$,

$$\frac{d(I/I_0)}{dV_a} \approx \left(\frac{\pi Ln^3 r_{41}}{\lambda_0} \right)^2 E_0 \frac{dE_0}{dV_a} \quad (16b)$$

Using equation (15), we find

$$\frac{dE_0}{dV_a} = \frac{e}{\varepsilon} \frac{T}{2w_g} N_2 \left[1 + b_2 + \frac{b_2 T^2}{W^2} \right] \frac{dW}{dV_a} \quad (17a)$$

$$\frac{dW}{dV_a} = \frac{1}{2W} \frac{2\varepsilon}{eN_2} \quad (17b)$$

Using equations (17a,b) and (9) in (16b), we find

$$\frac{d(I/I_0)}{dV_a} = \frac{e}{\varepsilon} N_2 \left(\frac{T}{2w_g}\right)^2 \left(\frac{\pi Ln^3 r_{41}}{\lambda_0}\right)^2$$

$$\times \left[(1 + b_2)^2 - \frac{T}{W}\left(1 + 2b_2 - \frac{N_1}{2N_2}\right)(1 + b_2)\right.$$

$$\left. + \frac{T^2}{W^2} 2b_2 (1 + b_2) + \frac{T^3}{W^3} b_2 \left(1 + 2b_2 - \frac{N_1}{2N_2}\right) + \frac{T^4}{W^4} b_2^2\right] \quad (18)$$

For a waveguide with the refractive indexes and dimensions of our experimental sample and in the 1.55- to 1.65-μm wavelength range b_2 is found to be 0.8 to 0.9. Using $T = 0.18$ μm, $N_1 = 5\times10^{16}$ cm^3, $N_2 = 5\times10^{17}$ cm^3 at $V_a = 2$ V, $W = 0.2$ μm, and at $V_a = 6$V, $W = 0.22$ μm. The term in square brackets in equation (18) is equal to 3.35 at $V_a = 2$ V and 2.84 at $V_a = 6$ V. This shows the slope to be substantially constant over the range of voltage of interest for our experiment. We thus use 3.1 as the average value of the bracketed term of equation (18). With this convenient approximation, the expression for the electro-optic coefficient r_{41} becomes

$$r_{41} = \left(\frac{\lambda_0}{\pi Ln^3}\right)\left(\frac{2w_g}{T}\right)\sqrt{\left(\frac{\varepsilon}{(3.1)\ eN_2}\right)\left(\frac{d(I/I_0)}{dV}\right)} \quad (19)$$

The validity of this treatment is born out by our observation of a linear increase of electro-optic signal with V_a (see fig. 5). Equation (19) allows

the direct computation of the electro-optic coefficient from a measurement of the slope of the electro-optic signal. Numerically we have:

$$
r_{41} = \begin{cases} 7.33 \times 10^{-12} \sqrt{\dfrac{d(I/I_0)}{dV}} \quad (m/V) & \begin{cases} \lambda_0 = 1.65 \ \mu m \\ n = 3.45 \end{cases} \\[30pt] 6.55 \times 10^{-12} \sqrt{\dfrac{dI/I_0}{dV}} \quad (m/V) & \begin{cases} \lambda_0 = 1.54 \ \mu m \\ n = 3.50 \end{cases} \end{cases}
$$

E. FRANZ-KELDYSH EFFECT

The Franz-Keldysh effect is described as a change in absorption due to an electric-field-induced shift in the band edge. This effect can become very strong as the wavelength approaches the bandgap. In general, the change in absorption for λ_0 near the band edge is expected to be an exponential function of the applied field in the crystal.

We are able to observe the electroabsorption in the near-field image of the light exiting from the modulator. Indeed, by the use of a slit we measure the electroabsorption at the peak of the near-field image of the waveguide mode when the bandgap of the modulator is at 1.23 μm and that of the source at 1.30 μm. For this wavelength, $w_g = 0.33 \ \mu m$ and the waveguide mode more nearly fills the active region than in the longer wavelength measurements. Here a simple approximation to the overlap integral is appropriate. We use the direct average

$$
E_0 = \frac{E_T + E_m}{2} \left(\frac{T}{2w_g} \right) + \frac{E_T}{2} \left(\frac{W - T}{2w_g} \right) \tag{20}
$$

The first term is the overlap in region I and the second term, the overlap in region II. Using equations (7), (8), and (9) in equation (20), we obtain the simple result

$$E_0 = \frac{V_a + V_{BI}}{2\omega_g} \tag{21}$$

We may thus write the fractional change in transmission for the Franz Keldysh effect as

$$I/I_0 = K_f \left[1 + \exp \left(-\alpha_f L \; \frac{V + V_{BI}}{2\omega_g} \right) \right] \tag{22}$$

We define a convenient Franz-Keldysh coefficient α_f which has the dimension $(V/cm)^{-1} \; cm^{-1}$. This is the absorption coefficient in inverse centimeters per unit applied electric field in volts per centimeter. With this definition the modulator length L and ω_g are in centimeters.

III.   EXPERIMENTAL METHOD

Our sample consisted of an InGaAsP laser mounted transversely on a copper heat sink as shown in Figure 3. Both facets are accessible. The sample is pulsed in back-bias and is used as a waveguide modulator to study the electro-optic effects. The InGaAsP active layer of the sample used in these studies has a bandgap wavelength of 1.230 μm. We refer to this sample as the modulator.
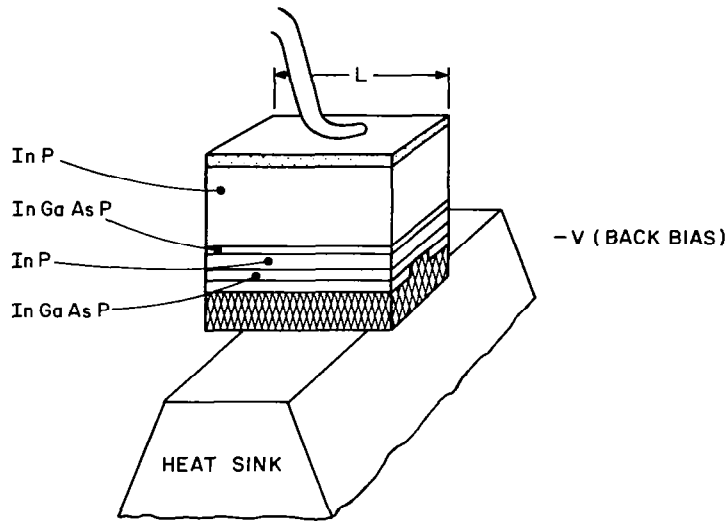
Figure 3.   Schematic diagram of the modulator showing the heat-sink mounting and N side electrical contact wire.

The experimental arrangement is shown in Figure 4. Light from a quaternary laser is focused onto one facet of the modulator with a 20-power microscope lens. For the electroabsorption measurements, the light emerging from the modulator is brought to a focus at the plane of a slit placed in front of a detector. A 10-power microscope objective is used for this purpose. The slit and detector can be scanned in the x direction. For the much weaker linear electro-optic effect measurements a polarization analyzer is placed between the slit-detector and the 10-power objective; also, the slit is opened to allow all the light in the modulator image to enter the detector.

Figure 4. Block diagram of experimental arrangement. Polarization
            analyser removed for absorption measurements. Modulator
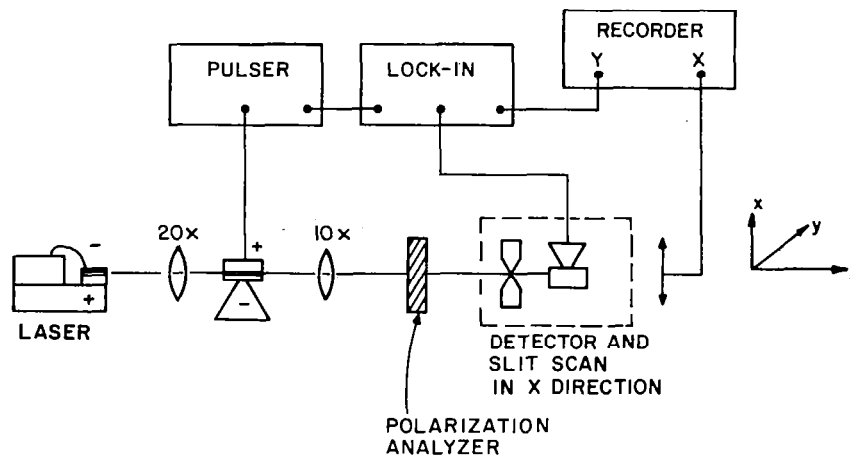   bandgap wavelength = 1.230 μm.

The source laser may be rotated around the z axis so that the polarization of the light entering the modulator may be varied. When the laser and modulator planes are parallel, TE modes will be excited in the modulator (E vector parallel to y axis). If the planes are at right angles, TM modes are excited (E vector parallel to x axis).

For the linear electro-optic effect measurement, the plane of the laser and hence the E vector of the light is rotated to a position which is 45° to the y axis. In this measurement the polarization analyzer is used, and it is rotated so that with no voltage applied to the modulator, no light passes through the analyzer. The modulator is then pulsed in back bias and the output measured directly from the lock-in amplifier as a function of the pulse voltage.

The detector-lock-in amplifier chain is calibrated in terms of percentage modulation by pulsing the source laser on and off at the same pulse repetition rate and duty cycle as is subsequently applied to the modulator. Linear electro-optic effect measurements are made with two different source lasers, one at 1.65 μm and the other at 1.54 μm. These wavelengths are sufficiently far from the 1.23-μm bandgap wavelength of the modulator to reduce the Franz Keldysh effect to values sufficiently low to allow observation of the linear electro-optic effect.

For the observation of the Franz-Keldysh (electroabsorption) effect, a source laser at 1.298 μm is used. Here, the polarization analyzer is removed, and the slit is narrowed so that the near-field image of the modulator wave-guide mode can be scanned. The cw measurement of the waveguide mode is obtained directly, bypassing the lock-in amplifier, using the detector output to drive the y axis of the recorder. The slit-detector position is recorded on the x axis. The laser is operated cw.

Following the cw scan, the modulator is pulsed and the modulated near-field image scanned using the lock-in amplifier. The lock-in is calibrated as is done for the linear electro-optic effect. After the modulated image is scanned, the slit is positioned at the peak of the image and the pulse voltage varied to obtain the voltage dependence of the electroabsorption.

IV. EXPERIMENTAL RESULTS

The results of the linear electro-optic (Pockel's) effect measurements are shown in Figure 5. We plot I/I_0 as a function of applied (pulse) voltage when the laser junction plane is 45° to the modulator junction plane and the polarization analyzer is placed as described in the previous section. The circles are the data points for λ_0 = 1.54 μm and the squares are for λ_0 = 1.65 μm. As mentioned earlier, the modulator bandgap is 1.23 μm as found from photoluminescence measurement. For both cases the data points are well-fitted by a straight line. For λ_0 = 1.54, the slope $(d(I/I_0)/dV)$ is 4.67×10^{-4}/V. Thus, from equation (19) r_{41} = 1.41×10^{-13} m/V. At λ_0 = 1.65 the slope is 2.14×10^{-4}/V and r_{41} = 1.07×10^{-13} m/V.

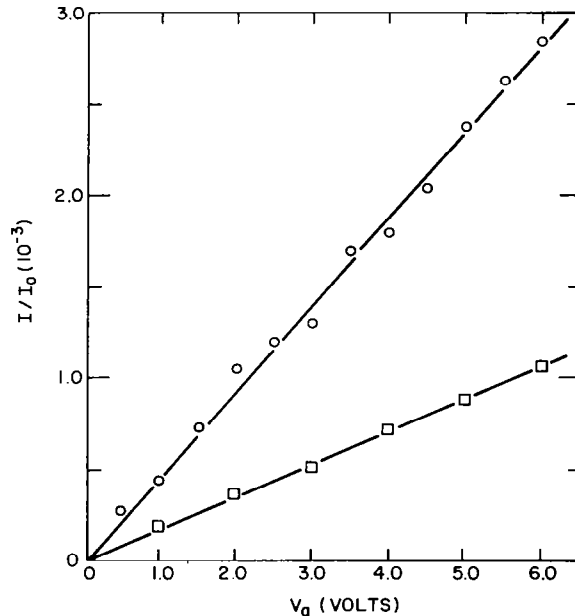Figure 5. Plot of fractional intensity variation of light passing through both modulator and polarization analyzer. Light entering modulator is polarized at 45° to waveguide plane. Analyzer is adjusted to extinguish light when no voltage is applied to modulator. Back bias increases as V_a increases. Circles (o): experimental points for λ = 1.54 μm; squares (□): experimental points for λ = 1.65 μm.

With a laser at λ_o = 1.3 μm, X-Y recorder tracings of the cw and self-modulated near-field images as described in Section V are given in Figure 6. The tracing of the modulated image is taken at V_a = -3 V (pulsed).

NEAR FIELD
IMAGE OF MOD. FACET
ZERO BIAS

INTENSITY (I)
INCREASING

NEAR FIELD
LOCK IN OUTPUT
MODULATOR PULSED
IN REVERSE BIAS
AT 3V

INTENSITY (I)
INCREASING
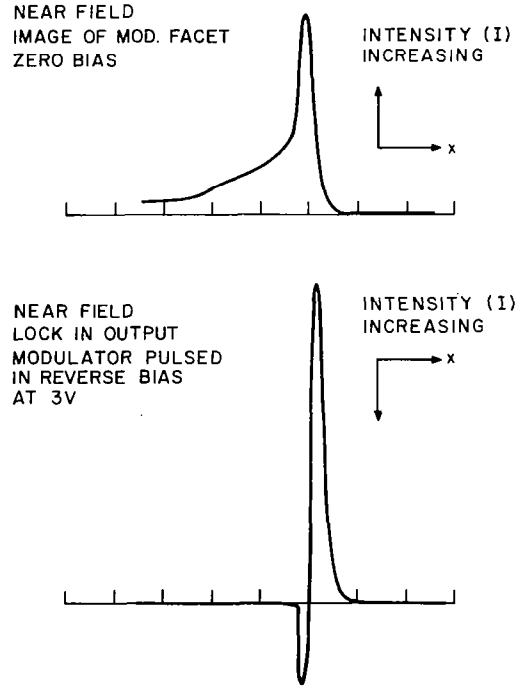
Figure 6. Top: X-Y recorder tracing of near-field of InGaAsP modulator waveguide under zero bias. Bottom: X-Y recorder tracing of modulated near-field intensity at reverse bias pulse voltage of 3 V. λ = 1.3 μm.

The fractional modulation I/I_0 with the slit set at the peak of the self-modulated near-field image is plotted against V_a in Figure 7. The circles are the data points for TE excitation and the triangles are points for TM excitation. In each case the solid lines are curves fitted using the theoretical expression [eq. (21)]. For the experimental values (L = 2×10^{-2} cm, V_{BI} = 1.35 V, λ = 1.298, and ω_g = 0.48×10^{-4} cm) we find

$$\alpha_f = 7.24 \times 10^{-4} \text{ cm}^{-1}/(\text{V/cm}) \text{ and}$$
$$K_f = 0.551$$

18
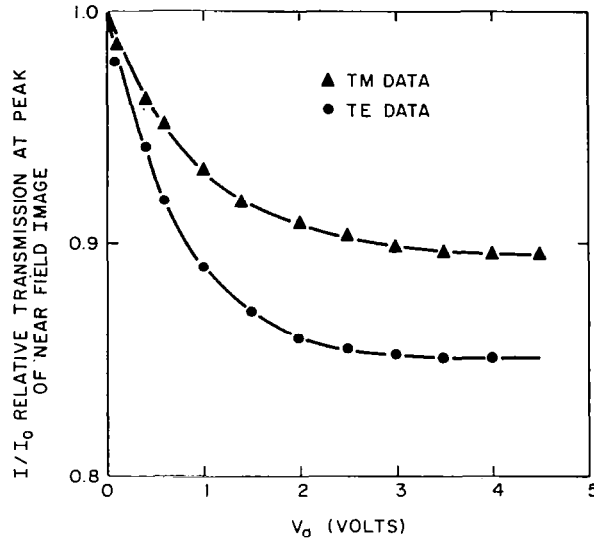
Figure 7. Plot of fractional transmission of modulator with slit placed at peak of modulated near-field intensity of Figure 6. Triangles (Δ): TM data (source laser junction plane perpendicular to modulator waveguide plane); circles (o): TE data (source and modulator planes parallel); solid curves fitted to data using equation (21), $\lambda = 1.3 \ \mu m$.

for the TE mode and

$$\alpha_f = 4.63 \times 10^{-4} \ cm^{-1}/(V/cm) \ \text{and}$$
$$K_f = 0.533$$

for the TM mode. For fields approximating those of our experiments ($E_0 \sim 2 \times 10^5 \ V/cm$) the Franz-Keldysh absorption coefficients are on the order of $100 \ cm^{-1}$. A summary of our results is given in Table 1.

TABLE 1. SUMMARY OF RESULTS

Modulator Bandgap Wavelength (μm)	Source Wavelength (μm)	Mode	r_{41} (m/V)	α_f cm^{-1}/(V/cm)
	1.65	TE	1.07×10^{-13}	--
	1.54	TE	1.41×10^{-13}	--
1.23		TE	--	7.24×10^{-4}
	1.30			
		TM	--	4.63×10^{-4}

V. DISCUSSION

The theoretical description of the effect of an applied voltage on the propagation of light in the waveguide formed by a quaternary layer as studied in this contract is in good agreement with the observations. For wavelengths (1.65, 1.54 μm) far away from the bandgap (1.23 μm) of the modulator the linear electro-optic effect may be observed and does indeed result in a linear voltage variation of light intensity transmitted through the polarization analyzer. This is clearly evident in the plots of Figure 5. Using the slope of this plot in conjunction with the theory, we obtain the electro-optic coefficient r_{41} for the InGaAsP layer. The observed value of $r_{41} \sim 10^{-13}$ m/V is only about ten percent of the r_{41} of GaAs (1.4×10^{-12} m/V). The error in the r_{41} measurements is difficult to assess without further work. Important physical constants for the quaternaries are still not available; of direct significance to our work is the precise value of the index of refraction, the third power of which enters as a factor in the expression for r_{41} [eq. (19)]. In addition, the value of the dielectric constant (ε) enters through equation (19) and in the constant term of equation (15). We feel that the uncertainties in the values of n and ε are of the order of 10% and must be considered to give uncertainties in the value of r_{41} of ±30%.

A further source of error lies in the interference of the Franz-Keldysh effect with the Pockel's effect measurements. At the longer wavelengths, voltage-dependent intensity changes on the order of 10 to 20% were observed without the use of the polarization analyzer. We take this as an indication of electroabsorption. The data presented for the linear electro-optic effect has been corrected for absorption. It is not fully clear at this time how the two effects should be separated at wavelengths where both are significantly present. We feel that additional study is warranted to clearly resolve this problem. In many conceivable applications of quaternary layers in integrated optics, it is likely that wavelengths may be used at which both the Pockel's effect and the Franz-Keldysh effect are important. The simple question as to whether, in any given application, the effects are additive or not remains to be answered.

The relatively small value of the electro-optic coefficient as compared to that of GaAs is certainly disappointing. However, r_{41}, is still of sufficient

magnitude to allow quaternary layers to be used in many of the waveguide electro-optic devices that have been reported so extensively in the literature (ref. 8). In particular, optical directional coupling modulators with attractively small dimensions (<1 mm) could be realized with these materials.

The Franz-Keldysh measurements gave high values of electroabsorption. The variation of α_f with light polarization is expected (ref. 3). The agreement of the experimental variation of transmitted light as a function of voltage with our theoretical description is excellent. This approach should enable design of electroabsorption-based waveguide devices to proceed in a reasonably simple manner. We feel that the measurement precision is on the order of 10% at 1.23 μm. As mentioned earlier, in the intermediate range of wavelengths (as compared to the modulator bandgap) observations are complicated by the interaction of the Franz-Keldysh effect on the Pockel's effect measurement and require further study.

VI. CONCLUSION AND SUMMARY

We have made the first measurements reported to date of the electro-optic coefficient, r_{41}, of InGaAsP. We have also measured a coefficient which characterizes the electroabsorption of these layers. This material is important in the production of lasers, LEDs, and detectors in the 1.2- to 1.7-μm range which has become attractive for optical communications. Since InGaAsP is not available in bulk, we have originated techniques to measure the small electro-optic coefficient in the thin film. Our measurements and theoretical description are important in assessing the potential for the use of quaternary layers in electro-optic waveguide applications. Such devices will be of use in signal processing in the 1.2- to 1.6-μm wavelength region. The small but significant value of r_{41} (10^{-13} m/V) will allow the implementation of devices such as directional coupler switches and modulators. The relatively high value of electroabsorption we observe is also encouraging for the production of high-speed modulators.

REFERENCES

1. D. Z. Tsang, J. N. Walpole, S. H. Groves, J. J. Hsieh, and J. P. Donnelly: Intracavity Loss Modulation of GaInAsP Diode Lasers. Appl. Phys. Lett., vol. 38, no. 2, 1981, pp. 120-122.

2. F. K. Reinhart: Electroabsorption in $Al_y Ga_{1-y} As$-$Al_x Ga_{1-x} As$ Double Heterostructures. Appl. Phys. Lett., vol. 22, no. 8, 1973, pp 372-374.

3. R. H. Kingston: Electroabsorption in GaInAsP. Appl. Phys. Lett., vol. 34, no. 11, 1979, pp. 744-746.

4. G. H. Olsen, C. J. Nuese, and M. Ettenberg: Low-Threshold 1.25-μm Vapor-Grown InGaAsP cw Lasers. Appl. Phys. Lett., vol. 34, no. 11, 1979, pp. 262-264.

5. G. H. Olsen and T. J. Zamerowski: Progress in Crystal Growth and Characterization, Vol. II. B. R. Pamplin, ed., Pergamon, London, 1980.

6. S. M. Sze: Physics of Semiconductor Devices. Wiley-Interscience, New York, 1969.

7. E. Garmire in Integrated Optics. T. Tamir, ed., 2nd Ed., Springer Verlag, New York, 1979, page 279 et seq.

8. J. M. Hammer: Ibid, Chapter 4, p. 139.

1. Report No. NASA CR-3521	2. Government Accession No.	3. Recipient's Catalog No.
4. Title and Subtitle STUDIES OF SINGLE-MODE INJECTION LASERS AND OF QUATERNARY MATERIALS. VOLUME II — MEASUREMENT OF ELECTRO-OPTIC EFFECTS IN InGaAsP JUNCTION WAVEGUIDES		5. Report Date April 1982
		6. Performing Organization Code
7. Author(s) Jacob M. Hammer		8. Performing Organization Report No. PRRL-81-CR-29 (II)
9. Performing Organization Name and Address RCA Laboratories Princeton, NJ 08540		10. Work Unit No.
		11. Contract or Grant No. NAS1-15440
12. Sponsoring Agency Name and Address National Aeronautics and Space Administration Washington, DC 20546		13. Type of Report and Period Covered Contractor Report 2-4-80 to 5-15-81
		14. Sponsoring Agency Code

15. Supplementary Notes

16. Abstract

We have measured both the linear electro-optic (Pockel's) effect and electroabsorption (Franz-Keldysh effect) in waveguiding junctions of InGaAsP. With our data and a field overlap theory, the electro-optic coefficient r_{41} is found to be $0.1-0.14\times10^{-12}$ m/V at $\lambda = 1.54 - 1.65$ µm. To the best of our knowledge this is the first reported measurement of the electro-optic coefficient for InGaAsP.

We have also measured the electroabsorption and found a value on the order of 7×10^{-4} cm^{-1}/(V/cm) or approximately 100 cm^{-1} for fields of 2×10^{5} V/cm at $\lambda \sim$ 1.3 µm. All measurements were made on a quaternary film with a bandgap wavelength of 1.23 µm.

Because of the rapid commercial introduction of quaternary lasers, LEDs, and detectors to take advantage of large optical fiber bandwidths and low losses in the 1.2- to 1.7-µm region, these measurements are significant in providing some of the basic physical constants needed to design modulators and switches capable of operating at microwave frequencies in this wavelength region.

17. Key Words (Suggested by Author(s)) Single-mode injection lasers Quaternary materials Electro-optic effects InGaAsP junction waveguides Constricted double-heterojunction laser		18. Distribution Statement Unclassified – Unlimited Subject Category 34	
19. Security Classif. (of this report) Unclassified	20. Security Classif. (of this page) Unclassified	21. No. of Pages 29	22. Price A03